Essential Readings in Light Metals: Cast Shop for Aluminum Production.
Edited by John F. Grandfield and Dmitry G. Eskin.

NUMERICAL SIMULATION OF DC CASTING; INTERPRETING THE RESULTS OF A THERMO-MECHANICAL MODEL

Wim Boender, André Burghardt, Erik Paul van Klaveren, and Jan Rabenberg
Corus RD&T; P.O. Box 10,000; 1970 CA IJmuiden; The Netherlands

Keywords: Aluminium alloy, DC casting, Cold cracking, Thermo-mechanical model

Abstract

A few problems impede the efficiency of DC casting. Cold cracking, which occurs when thermally induced stresses locally exceed the tensile strength, is one of these problems. Especially, hard alloys like AA2000 and AA7000 alloys are prone to cold cracking. To gain insight into the mechanical behaviour of an ingot during casting, Corus RD&T developed a thermo-mechanical model. This numerical model simulates the evolution of temperatures, stresses, and strains inside the ingot as a result of the casting parameters, the cooling conditions, and the alloy's properties. A triaxial state of stress is shown to develop almost everywhere in the solid ingot. Interpreting these results, two approaches are reciprocally used to estimate the likelihood that a cold crack will form. In one approach, the principal stresses are assessed, yielding insight into the locations and directions of cracks. The other approach is based on energy, i.e. on the fracture toughness K_{Ic}. It provides insight into possible ways to avoid cold cracks, e.g. by pointing out that internal defects, like inclusions or pores, should be smaller than the critical crack length. The findings will be illustrated with results for the DC casting of an Al - 4.5% Cu alloy.

Introduction

The manufacture of aluminium products starts with the casting of ingots that are subsequently rolled to plate or sheet. Plates and sheets are used for a wide range of products, for example aeroplanes and beverage cans. The most widely used casting technique is direct chill (DC) casting, which is a semi-continuous process. DC casting was invented in the 1930s [1,2]. Subsequently, it was introduced into cast houses. Experiences after its introduction taught that softer alloys could be cast with no trouble but that high-strength alloys for the aerospace industry like 24S, the ancestor of today's alloy AA2024, were prone to cracking. Both cold cracking and hot tearing occurred. These vexing problems were overcome, and DC casting became the dominant method in cast houses.

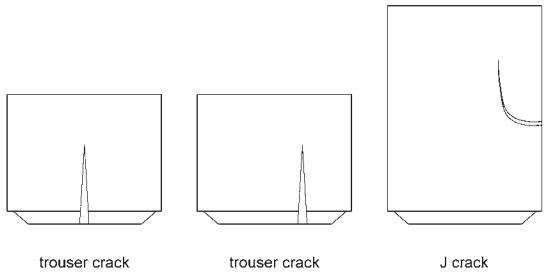

Figure 1. Types of cold cracks

Various types of cold cracks may occur in an ingot. Well known types are the trouser crack and the J crack shown by Figure 1 [3]. When a new high-strength alloy or a new and larger ingot format was introduced, these cracks sometimes reappeared. Employing various methods, these problems were usually solved [4, 5]. In the 1990s, numerical simulations of the mechanical behaviour of an ingot during casting were added to the tools that are used to solve these problems [6]. Here, the interpretation of the results of such simulations to assess the likelihood of cold cracking is discussed. Besides the mechanical stresses, these simulations can also describe phenomena like butt curl and pull-in of the rolling face [7, 8].

Thermo-mechanical model

A model that simulates numerically the thermal and mechanical phenomena in an ingot is called a thermo-mechanical model. That is to say, it produces temperatures, stresses, and strains, as functions of time and place. The thermal part of this numerical model calculates the temperature fields in both the ingot and the bottom block. Its mechanical part computes for the ingot the stresses, the strains, and the deformations that the shrinkage of the solidified metal causes. The model also takes into account the interaction between the butt curl and the heat transfer at the butt.
Corus RD&T (formerly Hoogovens R&D) developed its own thermo-mechanical model. Its first application was the simulation of the EM casting of AA3104 ingots [9]. Subsequently, it was used in the EMPACT project [10]. Moreover, it was successfully employed several times to improve the casting operations in the plants of Corus Aluminium. The model, whose further improvement is an ongoing process, has been set up in the finite element package MSC.Marc.

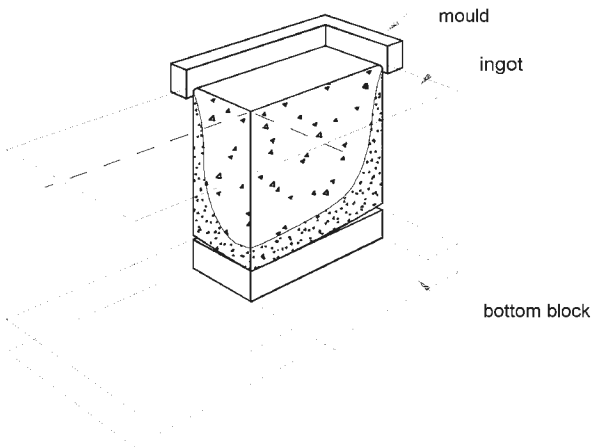

Figure 2. Mould, ingot and bottom block

Because of symmetry, only a quarter of the ingot has to be simulated. Figure 2 shows a perspective drawing of this quarter. In the model, the mould moves upwards, whereas both the ingot and the bottom block remain in the same position. Both the position of the meniscus and the thermal boundary conditions on the sides of the ingot are linked to the upwards moving mould. All elements of the ingot are present in the model from the start, but they are only activated after the horizontal part of the meniscus has passed. A consequence of this set-up is that heat cannot flow through the horizontal part of the meniscus. It is as if there is an adiabatic boundary condition.
The temperatures in the thermal part of the model, and the stresses and strains in the mechanical part are described by partial differential equations: the unknowns are functions of both space and time. To solve these equations some form of approximation has to be applied. Here, the finite element method is used.

Input

To illustrate how the results of a thermo-mechanical model can be interpreted, the casting of an ingot of an Al - 4.5% Cu alloy was simulated. This alloy was chosen, as it is a representative of high-strength alloys.
The input of the model consists of the dimensions of the mould, the ingot, and the bottom block; the process parameters for the drop; the physical properties of the ingot and the bottom block; and the boundary conditions.

Table I. Process parameters

Process parameter	Value
width ingot	2000 mm
thickness ingot	510 mm
final length ingot	2000 mm
casting speed	60 mm/min
temperature melt	675 °C
flow rate cooling water	45 m^3/hr
temperature cooling water	20 °C
start temperature bottom block	20 °C

Table I gives an overview of the process parameters. The mould opening was more or less rectangular. The double curved bottom block was made from steel. The length of the ingot was limited to 2000 mm in the simulation, which gives a complete picture of the start-up. The flow rate of the cooling water per unit length of the mould opening and the drop rate were similar to the ones Hannart et al. [6] had used for casting AA2024.
A prerequisite for a numerical model of DC casting is information on the physical properties of the pertinent aluminium alloy. Furthermore, since temperatures change substantially during casting, these properties have to be known as functions of temperature. The same applies to the properties of the material of the bottom block. Table II lists the properties of the Al - 4.5% Cu alloy and the way in which these properties were approximated. In the thermo-mechanical model, the density was kept constant. The volumetric, and by consequence, linear contraction were taken into account via the coefficient of thermal expansion. A modified Ludwik equation was used to describe the thermo-mechanical behaviour of the material [17]. Hannart et al. [6] and Magnin et al. [18] also employed this equation. It predicts stress as a function of strain, strain rate, and temperature. The parameters in this equation depend on the temperature. The parameters that Delft University had measured for an Al - 4.5% Cu alloy in the as-cast condition were used [18].

Table II. Physical properties of the ingot

Property	Approximation	Reference
specific heat	AA2024	[11]
thermal conductivity	AA2024	[12]
density	AA2024	[13]
Thermal expansion coefficient	pure aluminium	[14]
solidification range	AA2024	[13]
latent heat of fusion	pure aluminium	[15]
Young's modulus	AA2024	[16]
Poisson's ratio	AA2024	[16]

The data on the thermal conductivity of steel, the material of the bottom block, were taken from [19]. Data on its specific heat and density were found in [15].
From top to bottom, the following four areas are distinguished at the vertical sides of the ingot and the bottom block: the vertical part of the meniscus, the primary cooling zone, the air gap, and the secondary cooling zone. The direct contact between ingot and mould occurs in the primary cooling zone. During the stationary phase of a drop, the ingot may partly detach from the mould. A falling film of water cools the ingot in the secondary cooling zone. Between these two zones exists an air gap, where the ingot is neither in contact with the mould nor with the cooling water. The heat transfer from the ingot's vertical sides to the cooling water in the secondary cooling zone was described with the relation that had been established in the EMPACT project [20, 21, 22].
At the butt of the ingot, there may either exist a contact between ingot and bottom block; a narrow gap between them, which is filled with air and vapour; or a wide gap, which is filled with cooling water. Based on the local distance between the butt and the bottom block, the model determined which situation occurred. At the sides of the bottom block, the same boundary conditions were used as at the sides of the ingot. The boundary condition for the butt of the ingot also applied to the top of the bottom block. The heat transfer coefficient at the base of the bottom block was 50 W/(m^2 K). It was assumed that the bottom block transferred its heat there to air with a temperature of 20 °C.

Output

Figure 3 shows the temperatures inside the ingot at a cast length of 1.88 m. It covers the same quarter of the ingot as shown in Figure 2. Figure 4 shows the normal stresses in the x-direction, i.e. the stresses perpendicular to the casting direction and parallel to the rolling face at the same instance. Tensile stresses are positive and compressive stresses are negative. It contains two pictures, which both show a quarter of the ingot. The picture on the left-hand side shows the inside of the ingot and the picture on the right its exterior. Each picture contains the ingot and the bottom block. Only the contours of the mould are sketched. It is shown in two positions: one at the start of the cast and one at the moment the figure pertains to. There are large tensile stresses in the x-direction in the lower interior part of the ingot, and there are large compressive stresses in the x-direction at the lower part of

the rolling face. The shell of the lower part of the ingot has already reached the temperature of the cooling water. However, the interior of the lower part is still hot. As the interior continues to cool down, it shrinks, which the rigid shell counteracts. The stress state in the lower part of the ingot results from a balance between tensile stresses in the interior and compressive stresses in the shell.

Figure 5 shows in the same way as Figure 4 the normal stresses in the y-direction, i.e. the stresses perpendicular to the casting direction and perpendicular to the rolling face. The left-hand picture shows that there are considerable tensile stresses in the y-direction in the lower interior part of the ingot, particularly near the corner between butt and narrow side. The right-hand picture shows that there are large compressive stresses in the y-direction on the narrow side. The explanation of the normal stresses in the y-direction in the lower part of the ingot is similar to the explanation of the normal stresses in the x-direction in that area.

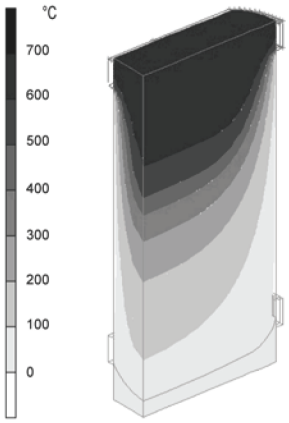

Figure 3. Temperatures

Figure 6 shows the stresses in x and y-direction at the surface just below the mould. Substantial tensile stresses occur at the top of both the rolling face and the narrow side. As the ingot leaves the mould, jets of cooling water hit its shell and this shell is cooled down rapidly. The material shrinks due to this cooling. However, the material below the impingement zone counteracts this shrinkage.

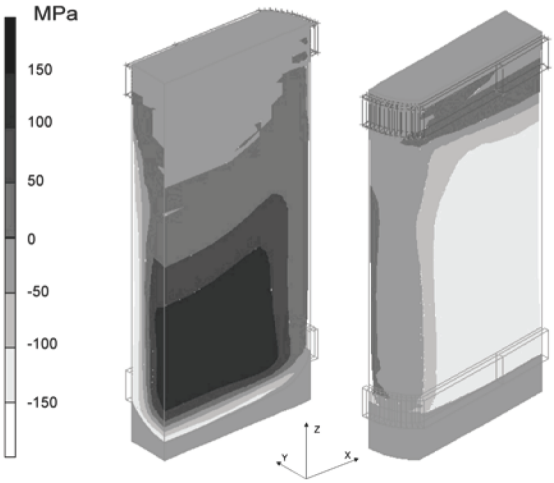

Figure 4. Normal stresses in x-direction

This counteraction causes compressive stresses in the areas below the impingement zone. These stresses can also be seen in Figure 4 and Figure 5. This demonstrates that the cooling of the shell in the impingement zone causes a stress state that can be explained qualitatively.

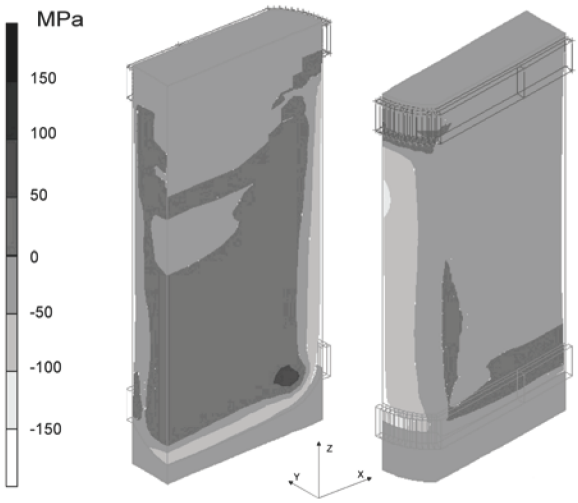

Figure 5. Normal stresses in y-direction

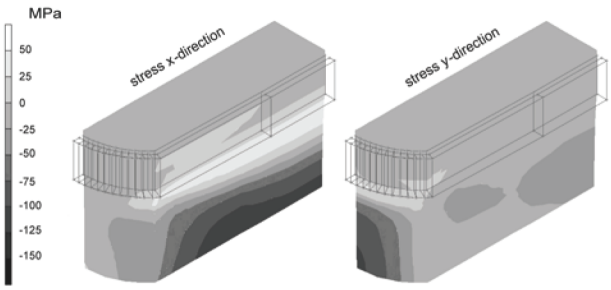

Figure 6. Stresses below the mould

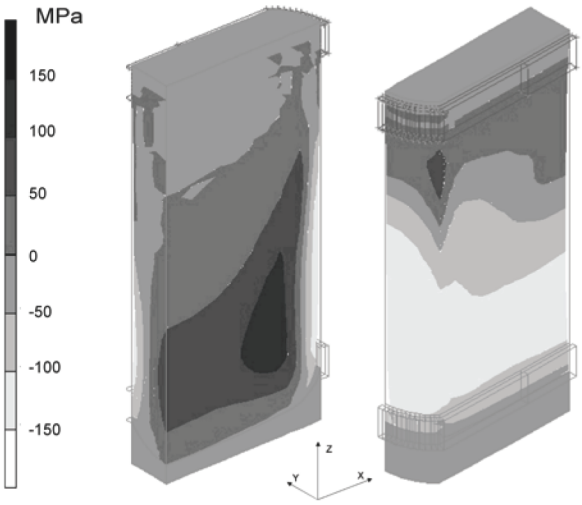

Figure 7. Normal stresses in z-direction

Figure 7 shows the normal stresses in the z-direction, i.e. the stresses parallel to the casting direction. The left-hand picture shows that there are large tensile stresses in the z-direction in the

lower interior part of the ingot. They occur notably close to the narrow side. The right-hand picture shows that there are large compressive stresses in the z-direction in the lower parts of both the rolling face and the narrow side. The explanation of the normal stresses in the z-direction in the lower part of the ingot, which Figure 7 shows, is similar to the one for the normal stresses in the x-direction. On the edge between the rolling face and the narrow side, an area with high tensile stresses in the z-direction can be seen. Contrary to the material that is near the centre of the rolling face or the narrow side, the material that is close to this edge loses heat to two sides. As a result, it cools down quicker and the rate at which the material shrinks is higher. This causes the tensile stresses in the z-direction.
Figure 4, Figure 5, Figure 6, and Figure 7 show the state of stress within the ingot. In the solidified part of the ingot, none of three normal stresses is negligible. Therefore, a real triaxial state of stress exists. Furthermore, the stress states in these figures can be qualitatively understood.

Failure criteria

Stress is a symmetric 3 × 3 tensor, which contains six scalar-like elements: three normal stresses and three shear stresses. This complicates the interpretation of the stresses in an ingot that is being cast to assess the likelihood of a cold crack. All the more, since the three normal stresses, which are shown above, were not negligible. Therefore, applying hypotheses on the strength, the triaxial stress state is converted into an imaginary uniaxial state that would have the same effect in the material. The pertinent imaginary stress is called ideal stress, σ_{id}.
This ideal stress is subsequently compared with the yield stress, σ_{YP}, or the tensile strength of a material, σ_{UTS}, which were established via tensile tests. This leads to a failure criterion, i.e. σ_{id}, should be less than either σ_{YP} or σ_{UTS}. The purpose of failure criteria is to predict or estimate the yielding or the actual rupture of machine parts and structural members. Here, such a criterion is used to assess whether an ingot is likely to crack.
A consequence of the symmetry of the stress tensor is that, at each point, three mutually perpendicular directions exist along which there are no shear stresses. These directions are called the principal stress directions, and the corresponding normal stresses are called the principal stresses. These principal stresses can be used in the definition of a failure criterion.

Equivalent von Mises stress

First, it was assumed that the ingot was ductile. Therefore, the theory of Huber and von Mises was used to calculate the ideal stress, which is called the equivalent von Mises stress [23, 24]. They proposed to use only the strain energy of distortion to determine yielding and failure of a material. According to their theory, yielding begins when this energy of a triaxial stress state reaches the value corresponding to the yield point in a simple tensile test. Here, the pertinent ideal stress was used to estimate the likelihood of cold cracking since it takes into account all elements of the stress tensor. This stress is defined as follows:

$$2\,\sigma_{id}^{\,2} = (\rho_1 - \rho_2)^2 + (\rho_2 - \rho_3)^2 + (\rho_3 - \rho_1)^2$$

where ρ_1, ρ_2, and ρ_3 are the principal stresses of the triaxial state of stress. It should be noted that ρ_1 is the maximum principal stress and that ρ_3 is the minimum principal stress.

Figure 8 shows the equivalent von Mises stress. The set-up of this picture is equal to the one of Figure 4. The equivalent von Mises stresses in Figure 8 reflect the stress states shown above. That is, there are large stresses in the interior and at the shell of the lower part of the ingot.
However, one issue calls for a further explanation. In two spots in the interior, the equivalent von Mises stress is almost zero. One of them coincides with the area with high tensile stresses in the y-direction. Given the definition of the equivalent von Mises stress, it becomes zero when the three principal stresses are equal. If all these principal stresses are compressive stresses, the situation is as if an infinitesimal cube is compressed by submersion in a liquid. In principle, this is not a dangerous situation. If, on the other hand, all principal stresses are tensile stresses, this cube may be torn apart. That is to say, such a stress state prevents plastic deformation [25]. Instead of a ductile fracture, it may cause a cleavage fracture. The fact that the equivalent von Mises stress is nearly zero does, therefore, not imply that no failure may occur. Hence, other ways to interpret the results of a thermo-mechanical model were investigated.

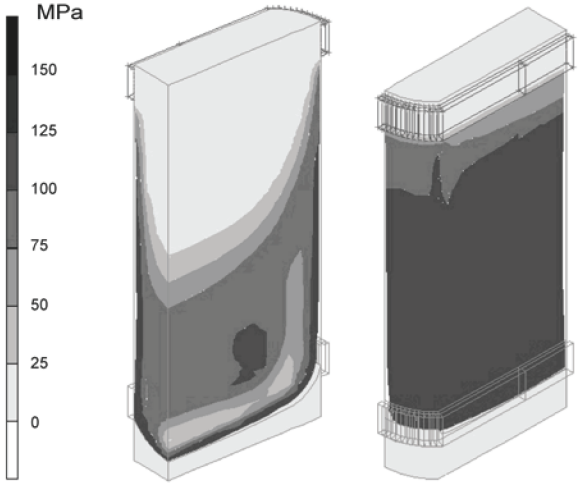

Figure 8. von Mises stress

Principal stresses

To gain more insight into the stresses within an ingot, the principal stresses and their directions were evaluated. Furthermore, this approach demonstrates what the application of the maximum normal stress criterion may bring. This criterion, which is also known as Rankine's theory, was assumed more applicable to brittle materials than the other theories [26]. It states that failure occurs when either the maximum principal stress reaches the uniaxial tensile strength or the minimum principal stress reaches the uniaxial compressive strength [24]. The application of this criterion to the DC casting of AA2024 was discussed in [6]. Chang and Kang [27] showed the distribution of the maximum principal stress for casting AA7050. Not only is its distribution shown here but also its direction.
Figure 9 shows the directions of the major principal stress for the ingot's interior, i.e. the wide symmetry plane, and its surface, i.e. the rolling face. The major principle stress equals ρ_1 if ρ_1 is greater than the absolute value of ρ_3, else it equals ρ_3. The major principal stresses are directed horizontally in the centre region.

Going towards the narrow side, these tensile stresses turn more and more to the vertical direction. Figure 10 shows the values of the major principal stresses for the interior and the surface of the ingot. Assuming cracks only occur in regions of large tensile stress, and that they propagate only perpendicularly to the tensile stress directions, one can conclude the following. Areas with a high probability of crack formation are found about 100 mm below the surface of the narrow side or a few 100 mm above the butt. The cracks near the narrow side would then propagate following a path that resembles J-cracks. Those near the bottom block would propagate upwards like trouser cracks. The observation of the directions of the major principal stresses, therefore, led to hypotheses for the start locations and the directions of trouser and J cracks.

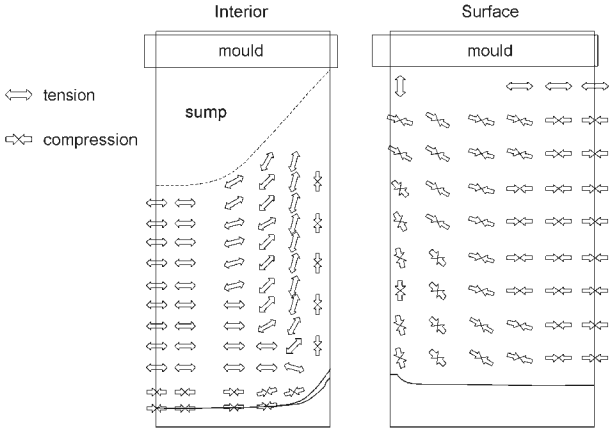

Figure 9. Directions of major principal stress

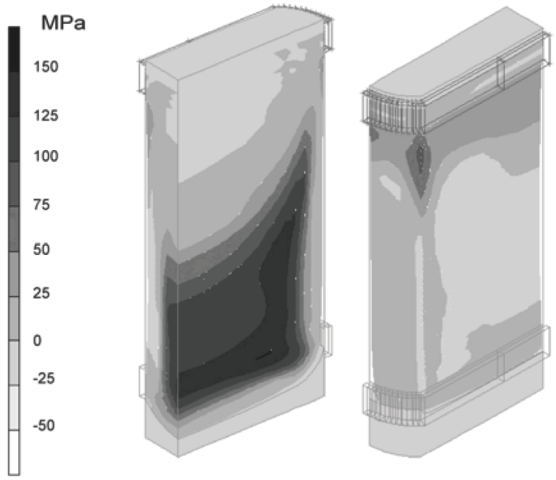

Figure 10. Major principal stresses

Fracture mechanics

The results of Chang and Kang [27] for the maximum principal stress when casting AA7050 can be compared with the tensile strength that Chang and others measured [27, 28]. The stresses appear to be less than the tensile strength; see also [3]. This finding complies with the experience of the authors. The fact that cold cracks nevertheless occur is, therefore, due to the presence of stress raisers.

To determine the effect of the size of an imperfection on an ingot's mechanical behaviour, fracture mechanics was applied. An existing crack propagates only if the total energy of the system decreases [29]. The elastic strain energy decreases as the crack extends. However, energy is needed to create the new crack surfaces and to bring about plastic deformation. Following this energy approach, the maximum size of an imperfection that can be tolerated under a certain loading can be determined. That is:

$$\sigma_c = \frac{K_{Ic}}{\sqrt{\pi a}} \qquad a_c = \frac{K_{Ic}^2}{\pi \sigma^2}$$

where K_{Ic} is the plane strain fracture toughness, σ is the tensile stress, a is half the length of the crack, and the subscript c stands for critical. Cracks that are longer than $2a_c$ grow unstoppably.

No data on the fracture toughness of an Al - 4.5% Cu alloy is available, but Chang et al. measured it for AA7050 in the as-cast condition at room temperature [27, 30]. Hence, their data is used to demonstrate the application of fracture mechanics. The minimum value of K_{Ic} they measured was 8.54 $MNm^{-3/2}$ [27]. Using this value, the critical crack lengths for AA7050 at a few tensile stresses were calculated. The selection of these stresses is based on the tensile stresses in Figure 10. Table III shows the results. For example, Gauckler et al. [31] mention the sizes of a few types of inclusions in aluminium. Especially oxide skins, whose maximum size may be 5 mm, may be greater than the critical crack length. Hence, they may cause cracks in areas with high stresses.

Table III. Critical crack lengths for AA7050

Stress	Half crack length
MPa	mm
50	9.29
100	2.32
150	1.03
200	0.58
250	0.37
300	0.26

Conclusions

The stresses in the x, y, and z-directions that the thermo-mechanical model predicted were compared with what one might expect on the basis of a physical reasoning. The results of the model were consistent with the outcome of this reasoning.

Assuming the ingot was brittle produced more information than the assumption that it was ductile. The directions of the major principal stresses demonstrated where cracks might be initiated, and how they might propagate. The application of fracture mechanics produced the critical crack size, i.e. from which minimum size cracks would grow. Internal defects, like voids and inclusions, should be smaller than this critical size. If imperfections are distributed homogeneously in an ingot, a large volume with high tensile stresses will contain more of them than a

small volume. Hence, in the former case, it is more likely that a crack will grow than in the latter. To avoid cracks it is, therefore, not only necessary to lower the stress levels but also to decrease the sizes of volumes with high stresses. The thermo-mechanical model is a tool to find ways to achieve this.

Acknowledgements

The authors would like to thank the supplier of MSC.Marc in Gouda, the Netherlands, for their support provided during the development of the thermo-mechanical model.
The usefulness of the thermo-mechanical model was honed when applying it to improve the processes in the cast houses of Corus Aluminium. Therefore, the authors are grateful for the pertinent discussions with their colleagues in these plants.
They are also grateful for the discussions with their colleagues Henk Vegter and Katja Mussert at Corus RD&T on the application of fracture mechanics to DC casting.

References

1. M.B.W. Graham and B.H. Pruitt, *R&D for Industry, A century of technical innovation at Alcoa* (Cambridge, UK: Cambridge University Press, 1990), 251-262.
2. W. Roth, "Stranggießen von Leichtmetall nach dem Wassergießverfahren", *Zeitschrift für Metallkunde*, 40 (1949), 445-456.
3. J. Du et al., "Computational Modelling of D.C. Casting of Aluminum Alloy Using Finite Element Method", *Light Metals 1998*, ed. B. Welch (Warrendale, PA, USA: TMS, 1998), 1025-1030.
4. R.P. Dieffenbach, "Practical Problems in Casting Aluminum D.C. Ingot", *Light Metals 1971*, ed. T.G. Edgeworth (New York, NY, USA: The Metallurgical Soc. of the AIME, 1971), 529-534.
5. D. Altenpohl, *Aluminium und Aluminiumlegierungen* (Berlin, BRD: Springer-Verlag, 1965), 123-127.
6. B. Hannart, F. Cialti, and R. van Schalkwijk, "Thermal Stresses in DC Casting of Aluminium Slabs: Application of Finite Element Model", *Light Metals 1994*, ed. U. Mannweiler (Warrendale, PA, USA: TMS, 1994), 879-887.
7. J.M. Drezet and M. Rappaz, "Modelling of Ingot Distortions during D.C. Casting of Aluminium Alloys" *Metallurgical and Materials Transactions A*, 27A (October) (1996), 3214-3225.
8. H.G. Fjær and E.K. Jensen, "Mathematical Modelling of Butt Curl Deformation of Sheet Ingots, Comparison with Experimental Results for Different Starter Block Shapes", *Light Metals 1995*, ed. J. Evans (Warrendale, PA, USA: TMS, 1995), 951-959.
9. H. Biel et al., "Prediction of Butt Curl during EM Casting of Aluminium Ingots", *Proceedings of ICAA-6*, Vol. 1, eds. T. Sato et al., (Tokyo, Japan: The Japan Institute of Light Metals, 1998), 363-368.
10. A. Burghardt et al., "A Numerical Study of the Influence of Geometry and Casting Conditions on Ingot Deformation in DC Casting of Aluminium Alloys", *Proc. of the Int. Conference on Modelling of Casting, Welding and Advanced Solidification Processes IX*, eds. P.R. Sahm, P.N. Hansen, and J.G. Conley (Aachen, BRD: Shaker Verlag GmbH, 2000), 25-33.
11. Y.S. Touloukian and E.H. Buyco, *Thermophysical Properties of Matter*, vol. 4 (New York, NY, USA: IFI/Plenum, 1970), 513.
12. R.E. Taylor et al., "Thermophysical properties of molten aluminium alloys", *High Temperatures-High Pressures* 30 (3) (1998), 269-275.
13. J.R. Davies et al., ed., *Metals Handbook*, vol. 2 (Materials Park, OH, USA: ASM International, 1990), 70-73.
14. Y.S. Touloukian et al., *Thermophysical Properties of Matter*, vol. 12 (New York, NY, USA: IFI/Plenum, 1975), 2.
15. E.A. Brandes and G.B. Brook, *Smithells Metals Reference Book* (Oxford, UK: Butterworth-Heinemann Ltd, 1992), 8-1; and 14-1 - 14-4.
16. J.A. Brammer and C.M. Percival, "Elevated Temperature Elastic Moduli of 2024 Aluminum Obtained by a Laser-Pulse Technique", *Experimental Mechanics*, 10 (6) (1970), 245-250.
17. M.L. Nedreberg, "Thermal Stress and Hot Tearing During the DC Casting of AlMgSi Billets" (Ph.D. Thesis, University of Oslo, Oslo, Norway, 1991), II-14 - II-31.
18. B. Magnin, L. Katgerman, and B. Hannart, "Physical and Numerical Modelling of Thermal Stress Generation During DC Casting of Aluminium Alloys", Conference on Modelling of Casting, *Welding and Advanced Solidification Processes VII* , eds. M. Cross and J. Campbell, (Warrendale, PA, USA: TMS, 1995), 303-310.
19. W. Beitz and K.-H. Küttner, eds., *Dubbel - Taschenbuch für den Machinenbau*, (Berlin, BRD: Springer Verlag, 1983), 1356.
20. I. Opstelten and J.M. Rabenberg, "Determination of the Thermal Boundary Conditions during Aluminum DC Casting from Experimental Data using Inverse Modelling", *Light Metals 1999*, ed. C.E. Eckert, (Warrendale, PA, USA: TMS, 1999), 729-735.
21. J. Zuidema jr, I.J. Opstelten, and L. Katgerman, "Boiling Curve Approach for Thermal Boundary Conditions in DC Casting", *Proc. of Int. Congress "Continuous Casting" Frankfurt am Main, BRD, 13 - 15 November 2000*, ed. K. Ehrke and W. Schneider, (Weinheim, BRD: Wiley VCH Verlag GmbH, 2000), 138-142.
22. J. Zuidema jr et al., "Secondary Cooling in DC Casting: Modelling and Experimental Results", *Light Metals 2001*, ed. J.L. Anjier, (Warrendale, PA, USA: TMS, 2001), 873-878.
23. S.P. Timoshenko, *History of Strength of Materials*, (New York, NY, USA: McGraw-Hill Book Co. Inc., 1953), 354-388.
24. S. Timoshenko, *Strength of Materials*, Part II, (Princeton, NJ, USA: D. van Nostrand Company Inc., 1958), 444-462.
25. D. Broek, *The Practical Use of Fracture Mechanics* (Dordrecht, The Netherlands: Kluwer Academic Publisher, 1989), 31-33
26. J.H. Faupel and F.E. Fisher, *Engineering Design*, (New York, NY, USA: John Wiley & Sons, Inc., 1981), 242-252.
27. K-M. Chang and B. Kang, "Cracking Control in DC Casting of High-Strength Aluminum Alloys", *Journal of the Chinese Institute of Engineers*, 22 (1) (1999), 27-42.
28. H-M. Lu, K-M. Chang and J. Harris, "Constitutive Modeling of High-Strength Aluminum Casting", *Light Metals 1997*, ed. R. Huglen, (Warrendale, PA, USA: TMS, 1997), 1091-1095.
29. M. Janssen, J. Zuidema, R.J.H. Wanhill, *Fracture Mechanics*, (Delft, The Netherlands: Delft University Press, 2002), 3-21.
30. J. Wan, H-M. Liu, K-M. Chang and J. Harris, "As-cast Mechanical Properties of High-Strength Aluminum Alloy", *Light Metals 1998*, ed. B. Welch (Warrendale, PA, USA: TMS, 1998), 1065-1070.
31. L.J. Gauckler et al., "Ceramic Foam for Molten Metal Filtration", *J. of Metals*, 37 (9) (1985), 47-50.